Effect of shear on the symmetric diblock copolymer/nanorod mixture: A dissipative particle dynamics study*

He Lin-Li(何林李)†, Zhang Rui-Fen(张瑞芬), and Ji Yong-Yun(季永运)

Department of Physics, Wenzhou University, Wenzhou 325035*, China*

(Received 16 December 2011; revised manuscript received 4 February 2012)

The phase behaviours of a lamellar diblock copolymer/nanorod composite under steady shear are investigated using dissipative particle dynamics. We consider a wide range of nanorod concentrations, where the nanorods each have a preferential affinity to one of the blocks. Our results suggest that shear not only aligns the orientations of the diblock copolymer templates and nanorods towards flow direction, but also regulates the distribution of the nanorods within the polymer matrix. Meanwhile, the shear-induced reorientation and morphology transitions of the systems also significantly depend on the nanorod concentration. At certain nanorod concentrations, the competitions between shear-induced polymer thinning and nanorods dispersion behaviours determine the phase behaviours of the composites. For high nanorod concentrations, no morphology transition is observed, but reorientation is present, in which the sheared nanorods are arranged into hexagonal packing arrays. Additionally, the orientation behaviour of nanorods is determined directly by the applied shear, also interfered with by the shear-stretched copolymer molecules.

Keywords: dissipative particle dynamics, shear, nanocomposites, orientation

PACS: 83.80.Uv, 78.67.Sc **DOI:** 10.1088/1674-1056/21/8/088301

1. Introduction

Recently, block copolymer/nanoparticle composites have attracted considerable attention as nanoscience and advanced engineering materials, since such polymer/particle mixtures can constitute ideal self-assembling systems for creating high-performance nanocomposites. The block copolymer (BCPs) can self-assemble into a variety of periodic mesoscale structures such as spheres, cylinders, and lamellae when cooled below a certain temperature (order–disorder transition temperature T_{ODT}).[1] Then, the self-assembled phases of BCPs can provide a "template" to organize the nanoparticles (NPs) into three-dimensional (3D) ordered arrays within the polymer matrix, such as nano-planes, -wires, or -spheres, and thereby tailors the properties of the composites. Conversely, the presence of particles is not passive and can also change both the orientation and the morphology of the copolymers' microdomains. Therefore, the final morphology of nanocomposites is determined by a complex interplay between entropy and enthalpy within the system. This interplay can be tuned by controlling the particle size, shape, concentration, surface properties, etc., which especially depends on the shapes of the NPs from isotropic to anisotropic.

Different from spherical NPs, the particles with nonspherical shape display anisotropic behaviour in optical and electric properties,[2,3] which results mainly from the additional orientation entropy. Especially, the nanorods (NRs) are concentrated since their properties depend on their transversal and longitudinal sizes. In organized NRs superlattices, it may be possible to simultaneously and independently optimize photoelectric properties by varying the rod diameter (such as band gap) and length (total absorption, cross section, or conductivity).[4] For example, Huynh *et al.*[5] blended inorganic NRs and organic polymers (P3HT) to fabricate solar cells that possessed greater efficiencies than conventional organic photovoltaic cells, since the long axis of the rod provided a continuous channel for transporting electrons, an advantage over spherical particles where electron hopping between particles is required. Hence, the exploration of methods of controlling the distribution and orientations of NRs in a polymer matrix, are conducive to the improvement of the photoelectric prop-

*Project supported by the National Natural Science Foundation of China (Grant Nos. 21074096 and 21104060).

†Corresponding author. E-mail: helinli155@163.com

© 2012 Chinese Physical Society and IOP Publishing Ltd

erties of nanocomposites.

Some recent studies, whether in experiment, in theory or in simulation, have focused on utilizing the self-assembly characteristics of block copolymers melts to regulate the phase behaviours of NRs in the polymer matrix.[6−8] Zhang *et al.*[6] experimentally described the phase behaviours of CdSe nanorods in a diblock copolymer template, PS-b-PMMA, with lamellar nanoscopic channels and cylindrical nanoscopic pores. By choosing the NR dimensions relative to the channel or pore width, they could control the orientations and lateral positions of the NRs.[6] In our previous simulation studies on diblock copolymers (DBCPs)/NRs mixtures, we varied parameters such as the affinity between the NRs and blocks, the NRs size and concentration, and we observed rich self-assembly structures of nanocomposites and peculiar phase behaviours of NRs within the polymer matrix. Those results can be further rationalized on the basis of the interplay between enthalpy involving interactions between blocks and NRs, and entropy involving the orientational entropy of NRs, the configurational entropy of the chains, and the spatial confinement of phase-separated domains.[8]

Most previous studies on BCPs melts or BCPs/NPs systems are limited to equilibrium conditions. However, the complex behaviours of these materials applied by external fields cannot be overstated, such as shear flow, given that the nonequilibrium conditions are commonly encountered in experiments and manufacturing processes. Especially for BCP melts, the shear flow has been regarded as an effective approach to producing favourable effects which include the inducements of long-range order and order–disorder or order–order structural transitions, as well as the orientation of self-assembled structures. Meanwhile for the nanocomposites, there is increasing interest in the studies on how the shear flow affects the dynamic behaviours of block copolymer/nanoparticle composites.[9−11] Mendoza *et al.*[10] experimentally utilized shear flow to fabricate 3D periodic ordered arrays of gold NPs in a spherical, cylindrical, or lamellar structure of PS-b-P4VP diblock. Compared with the case of BCPs/NPs systems subjected to shear flow, studies on the hybrid systems of block copolymers and nanorods under nonequilibrium conditions are comparatively rare, whether in experiment, in theory or in simulation.

Recently, we studied the microphase transitions of block copolymer/nanorod composites under shear flow, where the NR concentration is fixed to be lower than 15%.[12] We obtained the interesting results that the self-assembly of composites and phase behaviours of NRs in a polymer matrix not only are dependent on the shear flow, but are also significantly affected by the locations of NRs in phase domain. In the present work, we utilize the dissipative particle dynamics (DPD) simulations to investigate the effects of shear on the mixtures of symmetric DBCPs/NRs with a wider range of NR concentrations. Take the selective NRs into consideration, which have a preferential affinity to one of the blocks. With the increase of NR concentration, we first obtain the rich morphologies of block copolymer/nanorod composites without shear. Then, by applying a shear flow over a range of shear rate, we investigate the phase behaviours of the nanocomposites, also including the orientations and distribution of NRs in the polymer matrix. From these simulations we aim to address three questions, (i) how anisotropic NRs affect the self-assembly of DBCPs melts either in equilibrium (without shear) or in nonequilibrium (with shear) conditions; (ii) how the shear flow induces the orientation and morphology transition of the composite system, including the phase behaviours of NRs (i.e., the positional distribution and spatial orientation); (iii) how the NR concentration affects the morphology transition and rheological property of the system. Our ultimate goal is to elucidate the nonequilibrium conditions under which even greater control of the highly ordered arrays of NRs is realized.

2. Theory and model

The DPD method is typically considered as a coarse-grained simulation technique, in which the DPD 'beads' or particles represent a cluster of atoms or molecules. The pairwise interactive force acting on a particle i by the particle j contains three parts: conservative force ($\boldsymbol{F}_{ij}^{\mathrm{C}}$), dissipative force ($\boldsymbol{F}_{ij}^{\mathrm{D}}$), and random force ($\boldsymbol{F}_{ij}^{\mathrm{R}}$), and it is expressed as

$$\boldsymbol{f}_i = \sum_{i \neq j} (\boldsymbol{F}_{ij}^{\mathrm{C}} + \boldsymbol{F}_{ij}^{\mathrm{D}} + \boldsymbol{F}_{ij}^{\mathrm{R}}), \tag{1}$$

where

$$\boldsymbol{F}_{ij}^{\mathrm{C}} = a_{ij}\omega\left(r_{ij}\right)\hat{r}_{ij}, \tag{2}$$

$$\boldsymbol{F}_{ij}^{\mathrm{D}} = -\gamma\omega^2\left(r_{ij}\right)\left(\hat{r}_{ij}\cdot\boldsymbol{v}_{ij}\right)\hat{r}_{ij}, \tag{3}$$

$$\boldsymbol{F}_{ij}^{\mathrm{R}} = \sigma\omega\left(r_{ij}\right)\theta_{ij}\hat{r}_{ij}. \tag{4}$$

The conservative force $\boldsymbol{F}_{ij}^{\mathrm{C}}$ is a soft interaction potential within a certain cutoff radius r_{c}. a_{ij} is a maximum repulsion between beads i and j, $\boldsymbol{r}_{ij} = \boldsymbol{r}_i - \boldsymbol{r}_j$, and $r_{ij} = |\boldsymbol{r}_{ij}|$, $\hat{r}_{ij} = \boldsymbol{r}_{ij}/r_{ij}$. For the weight function $\omega(r_{ij})$, we adopt the commonly used form: $\omega(r_{ij}) = 1 - r_{ij}$ for $r_{ij} < 1$ and $\omega(r_{ij}) = 0$ for $r_{ij} \geq 1$. The other two forces ($\boldsymbol{F}_{ij}^{\mathrm{D}}$ and $\boldsymbol{F}_{ij}^{\mathrm{R}}$) each act as a heat source, which effectively combines to thermostat the system. $\boldsymbol{v}_{ij} = \boldsymbol{v}_i - \boldsymbol{v}_j$, and θ_{ij} is a randomly fluctuating variable with Gaussian statistics: $\langle\theta_{ij}(t)\rangle = 0$ and $\langle\theta_{ij}(t)\theta_{kl}(t')\rangle = (\delta_{ik}\delta_{jl} + \delta_{il}\delta_{jk})\delta(t-t')$. Also, the fluctuation–dissipation theorem requires that the friction coefficient γ and the noise amplitude σ are related by $\sigma^2 = 2\gamma k_{\mathrm{B}}T$, where k_{B} is the Boltzmann's constant and T is the temperature. Here we set $\gamma = 6.57$, so $\sigma = 3.63$.[13] The radius of interaction, the particle mass, and the temperature are all set to be unity, i.e., $r_{\mathrm{c}} = m = k_{\mathrm{B}}T = 1$. Additionally, for modeling polymers, the chains are constructed by connecting the adjacent particles via an extra spring force $\boldsymbol{f}_i^{\mathrm{s}} = \sum_j C\boldsymbol{r}_{ij}$, where the constant of C is 4.0.

For modeling the rigid NRs, referring to the approach taken by the previous studies,[8,14] it can be successfully constructed by a number of DPD beads (N_b) arranged in a straight line, with a fixed small distance (D_{b-b}) between consecutive beads, where the length of a rod is expressed equivalently as $L_{\mathrm{R}} = (N_b - 1) \times D_{b-b}$. In order to avoid undesired penetration of fluid particles into the NRs and overlap between NRs, the number density of the DPD particles in a nanorod is larger than that of the fluid. Here, we select $N_b = 6$ and $D_{b-b} = 0.3$. Then the range ratio of L_{R}/L_0 (NRs length/period width of DBCPs) is about 0.33,[8] comparable to the experimental range ratio of $L_{\mathrm{R}}/L_0 = 10$ nm$\sim$60 nm/60 nm=0.17$\sim$1.0.[6] Additionally, for the NR motion, a constraining routine is used to keep the inner particles aligned and equidistant during the simulation. In short, the forces on the DPD particles of a rod are converted into a net force on the two end DPD particles, and the equations of motion for these two DPD particles are solved, using the standard SHAKE routine to keep them at a fixed distance. The positions of the $N_b - 2$ intermediate DPD particles are then readily calculated by a linear interpolation at the end of each timestep.[14] The Newton equations for all particle positions and velocities are integrated by a modified version of the velocity Verlet algorithm in steps of $\Delta t = 0.04\tau$, where τ is the natural unit of time, defined as $r_{\mathrm{c}}\sqrt{m/k_{\mathrm{B}}T}$.

Our model system consists of the symmetric diblock copolymers (A_5B_5) and NRs (R). The number density of the fluid is $\rho = 5$, and then the repulsive parameter a_{ij} in Eq. (2) relates to the Flory–Huggins χ-parameter, via

$$a_{ii}\rho = 75k_{\mathrm{B}}T, \tag{5}$$

$$a_{ij} \approx a_{ii} + 1.45\chi_{ij} \quad (\rho = 5), \tag{6}$$

where the repulsion parameter between particles of the same type $a_{ii} = 15k_{\mathrm{B}}T$ correctly describes the compressibility of the water. Here, the values of a_{ij} between the three types of DPD beads (represented by A, B, and R), are given by $a_{AA} = a_{BB} = a_{AR} = 15$, and $a_{AB} = a_{RR} = a_{BR} = 30$. This choice of interactions $a_{AR} = 15$ and $a_{BR} = 30$ ensures the affinity between block A and NRs (i.e., A-selective NRs).

To impose the external oscillatory shear flow, we use the SLLOD (so named because of its close relationship to the Dolls tensor) algorithm so that the equations of motion are modified as follows:[15]

$$\dot{\boldsymbol{r}} = \boldsymbol{p}_i/m + \hat{i}\dot{\gamma}r_{yi}, \tag{7}$$

$$\dot{\boldsymbol{p}}_i = \boldsymbol{F}_i - \hat{i}\dot{\gamma}p_{yi}, \tag{8}$$

where $\boldsymbol{r}_i$ and $\boldsymbol{p}_i$ are the position and the momentum of particle i, respectively, $\hat{i}$ is the unit vector in the x-axis direction, and $\dot{\gamma} = \partial v_x/\partial r_y$ is the shear rate. The flow direction is parallel to the x axis, the y axis refers to the velocity gradient, and the z axis represents the transverse direction. Meanwhile, we employ the Lees–Edwards periodic boundary condition to maintain the steady and linear velocity gradient, wherein two opposing periodic images are incrementally moved in opposite directions consistent with the applied shear. The maximal value of shear rate used here is $\dot{\gamma} = 0.21$ in reduced units, which is not too large and can avoid the potential microturbulence, and even distortion.

One of the most important parameters characterizing rheological properties is the shear viscosity, directly related to the pressure tensor P, which is measured by[16]

$$P_{\alpha\beta} = \frac{1}{V}\left\langle \sum_i \frac{p_{i,\alpha}p_{i,\beta}}{m_i} \right\rangle + \frac{1}{V}\left\langle \sum_i \sum_{j>i} F_{ij,\alpha}^{\mathrm{C}} r_{ij,\beta} \right\rangle, \tag{9}$$

where α and β are the Cartesian indices. Shear viscosity in association with the only nonvanishing off diagonal component $P_{xy} = -P_{yx}$ is given by

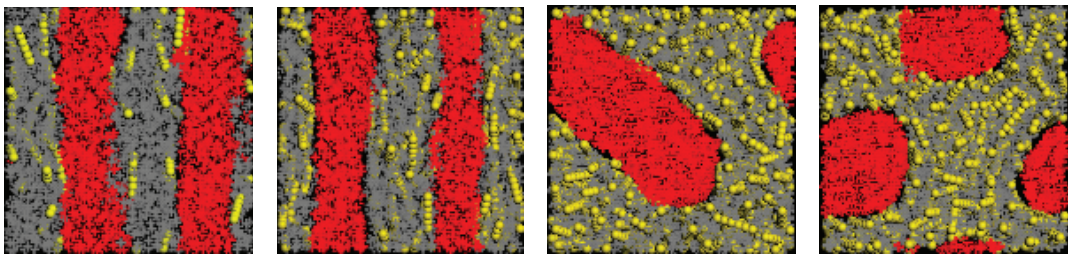
$$\eta = -\frac{P_{xy}}{\dot{\gamma}}, \tag{10}$$

where η is the non-Newtonian shear viscosity.

The simulations are performed in a cubic box of constant volume $V = 11 \times 11 \times 11$, with periodic boundary conditions applied in all three directions. The simulated systems contain $N_P = 6655$ polymer DPD beads and $\phi_{\rm R} N_P/(1-\phi_{\rm R})$ rod DPD beads for the number density $\rho = 5$, where $\phi_{\rm R}$ represents the NR concentration. Before being subjected to shear flow, firstly, A_5B_5 melts and NRs are randomly dispersed in the simulated box, the stable lamellar (LAM) phases of A_5B_5/NRs composites are obtained at least over 1.0×10^6 timesteps and independent of the initial state. Then, the equilibrium structures of the nanocomposites are placed in the direction transverse to the shear direction (i.e., the lamellar normal is parallel to the velocity direction), which is defined as the starting state. After application of the shear flow, the system evolves at least 2.0×10^6 timesteps in the nonequilibrium until a finally stable state is achieved.

3. Results and discussion

Firstly, we perform the simulations on the self-assembly of DBCPs/NRs systems without shear flow (i.e., under equilibrium conditions). With the increase of NR concentration, the system experiences a series of self-assembly phases, consistent with the previously obtained phase diagrams.[8] As shown in Figs. 1(a)–1(d), when $\phi_{\rm R} = 6\%$ and 15%, the ordered LAM structures are preserved. As $\phi_{\rm R}$ increases to 30% and even 35%, the LAM phase transits into ribbon and cylindrical structures shown in Figs. 1(c) and 1(d). The ribbon phase has been reported in previous studies,[8] which can be taken as a transient phase between lamellar and cylindrical morphologies. From Fig. 1, we can clearly see that the A-selective NRs are basically located within the compatible A domains. Obviously, an increase in the concentration of A-selective NRs, equivalently enhances the effective A block composition (f_A), therefore it causes the typical morphological transition from lamellar to cylindrical phase, corresponding to the theoretically predicted phase diagram for pure DBCPs melts.[17] These simulation results are also in agreement with those of mixtures of lamellar DBCPs and spherical NPs.[18] Then, the equilibrium structures of nanocomposites are placed in the direction transverse to the shear direction (i.e., the lamellar normal is parallel to the velocity direction), which is defined as the starting state. Imposed by the shear over a range of shear rates, the composites will undergo a series of orientation and morphology transitions. Here, our aim is to indicate the self-assembly processes of nanocomposites under shear. Here, we consider a wide range of NR concentrations, which is roughly divided into three regions: low NR concentration ($\phi_{\rm R} = 5\%$), moderate NR concentration ($\phi_{\rm R} = 15\%$ and 30%), and high NR concentration ($\phi_{\rm R} = 35\%$).



(a) (b) (c) (d)

Fig. 1. (colour online) Morphologies of DBCPs/NRs composites with $\phi_{\rm R} = 6\%$ (a), 15% (b), 30% (c), and 35% (d), where the NRs are preferentially located in A phase domains.

3.1. Low NR concentration

Here we investigate the effects of steady shear on the self-assembly of lamellar DBCPs and NRs mixtures, with a low NRs concentration of $\phi_{\rm R} = 5\%$. In Figs. 2(a1)–2(d1), we show simulation pictures of nanocomposites at different shear rates of $\dot{\gamma} = 0$, 0.01, 0.05, and 0.08, corresponding to the initial transverse LAM, parallel LAM, diagonal LAM, and perpendicular LAM morphologies, respectively. Similar to the case of DBCP melts under shear, an excellent agreement with experimental observations is found, that is, at low shear rates, the LAM phase preferentially aligns in the direction parallel to the shear direction, and at high shear rates, the LAM phase preferentially aligns in the direction perpendicular to

the shear direction.[19] Additionally, there is a transient LAM phase between parallel and perpendicular orientation, i.e., diagonal LAM structure (with the lamellae oriented in the shear direction but diagonally between a parallel and perpendicular alignment, see Fig. 2(c1)), which is also observed frequently in the case of steady shear.[20] As already discussed by Lísal and Brennan,[20] values of the potential energy and entropy production for the diagonal LAM phases lie between the corresponding values for the parallel and perpendicular lamellar phases. In these LAM phases of nanocomposites (Figs. 2(b1)–2(d1)), on the one hand, the NR orientation is highly sensitive to the imposed external field and immediately oriented to the flow direction, owing to the additional orientational entropy of the NRs; on the other hand, the NRs are exclusively distributed within the A phase domain, owing to the preferentially attractive interaction between NRs and A monomers of the blocks. The latter case is further confirmed by the densities of blocks A, B, and NRs, plotted in Figs. 2(b2)–2(d2). In a word, despite the block copolymers incorporated with anisotropic NRs being subjected to the shear, the interplay between entropy and enthalpy involving blocks A, B, and the affinity of NRs, still remains dominant for directing the equilibrium location of NRs within polymer matrix.

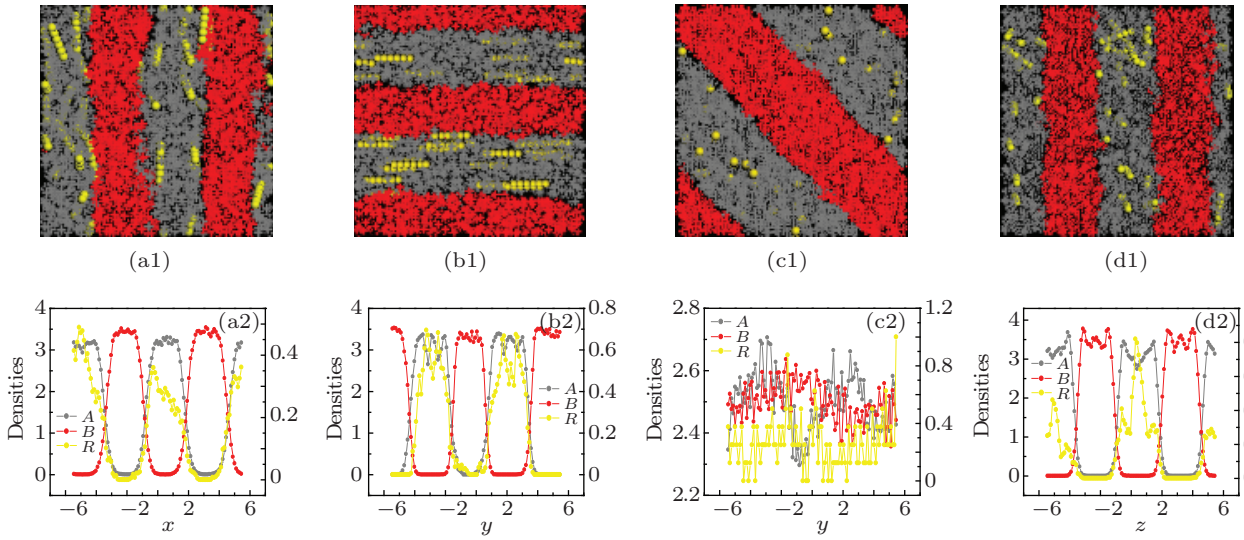


Fig. 2. (colour online) Morphologies and densities for DBCPs/NRs composites ($\phi_{\rm R} = 5\%$) at the shear rates of $\dot{\gamma} = 0$, 0.01, 0.05, and 0.08. Panels (a1)–(b2) show the views in the direction perpendicular to the shear direction, while panels (c2) and (d2) show the views in the direction parallel to the shear direction.

3.2. Moderate NR concentration

Then we turn to consider the systems of DBCPs/NRs with moderate concentrations of $\phi_{\rm R} =$ 15% and 30%. Before imposition of the shear flow, the corresponding initial structures of the nanocomposites are shown in Figs. 1(b) and 1(c). The imposed shear rate $\dot{\gamma}$ ranges from $\dot{\gamma} = 0$ to 0.21 in intervals of 0.005/0.01 at the lower rate and in interval of 0.02 at the higher rate. For $\phi_{\rm R} = 15\%$, figure 3 presents the typical simulated pictures of composites at shear rate $\dot{\gamma} = 0$, 0.01, 0.03, 0.05, 0.06, 0.09, 0.13, and 0.21, corresponding to the transverse LAM, parallel LAM, diagonal LAM, ribbon, cylindrical, ribbon, diagonal LAM, and perpendicular LAM structures, respectively, where NRs are located in A domains. From Fig. 3, we can clearly observe that the commonly shear-induced reorientations of transverse-to-parallel at low shear rates from $\dot{\gamma} = 0.001$ to 0.02 in Fig. 3(b), and transverse-to-perpendicular at high shear rates from $\dot{\gamma} = 0.15$ to 0.21 in Fig. 3(h). A transverse-to-diagonal reorientation of lamellae takes place at $\dot{\gamma} = 0.03$ and $\dot{\gamma} = 0.13$ shown, respectively, in Figs. 3(c) and 3(g) where the diagonal LAM (i.e., with the lamellae oriented in the shear direction but diagonally between a parallel and perpendicular alignment) can be taken as a transient phase between parallel and perpendicular LAM.[20] Interestingly, besides the reorientations in lamellae, the shear-induced morphology transitions of lamellae-to-ribbon and lamellae-to-cylinder appear at intermediate shear rates from $\dot{\gamma} = 0.05$ to 0.09 shown in Figs. 3(d)–3(f). Compared

with the case of nanocomposites with $\phi_R = 5\%$, the shear not only aligns the orientation of LAM along the flow direction, but also induces a series of morphology transitions of DBCPs/NRs composites. The latter contribute to the increase of A-selective NR concentration. Overall, figure 3 suggests that the shear-induced phase behaviours of mixtures experience a symmetrical and reversible process: from lamellar to ribbon to cylindrical phase with $\dot{\gamma}$ increasing from 0.01 to 0.06 shown in Figs. 3(b)–3(e), and then inversely, from cylindrical to ribbon to lamellar structure with $\dot{\gamma}$ increasing from 0.06 to 0.21 shown in Figs. 3(e)–3(h). These results are similar to the symmetric phase transitions caused by the block composition f, corresponding to the phase diagram of diblock copolymer melts,[17] suggesting that within a certain range of selective NR concentrations, which are subjected to shear flow, the effective block composition (f_{eff}) in composites can be equivalently influenced, thereby causing the phase transitions between lamellae and cylinder, which will be illustrated by the NR distribution in the polymer matrix.

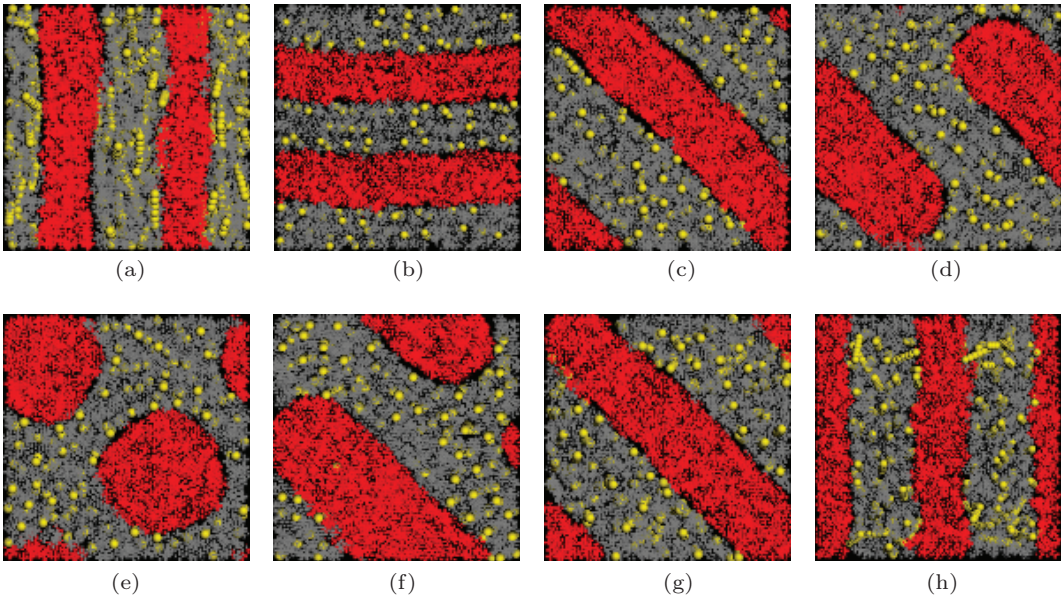


Fig. 3. (colour online) LAM reorientations and phase transitions of DBCPs/NRs composites ($\phi_R = 15\%$) at $\dot{\gamma} = 0$ (a), 0.01 (b), 0.03 (c), 0.05 (d), 0.06 (e), 0.09 (f), 0.13 (g), and 0.21 (h). Panel (a) shows the view of the initial lamellar structure in the direction perpendicular to the shear direction, while panels (b)–(h) show the views in the direction parallel to the shear direction.

The positional distribution of particles within the polymer matrix can be measured by the pair correlation function $g(r)$, which is related to the probability of finding the position of a particle at a given distance from another particle. For short distances, this is related to how the particles are packed together; for large distances, it is related to the density—a more dense system has more particles. Therefore, the pair correlation function $g(r)$ is normalized by the density and defined as[21]

$$g(r) = \frac{V}{N^2}\left\langle \sum_i \sum_j \delta(r - r_{ij}) \right\rangle, \tag{11}$$

where N is the number of particles, $\delta(r)$ is the Dirac delta function, and $\langle * \rangle$ means the ensemble average. Here, for the case of NRs well oriented to shear direction (i.e., x axis), we calculate the two-dimensional (2D) pair correlation function $g(r_{yz})$ by counting the position of the rod head-particle projected in the yz-plane. The pair correlation function $g(r_{yz})$ at different shear rates of $\dot{\gamma} = 0.01$, 0.03, and 0.06 are displayed in Fig. 4, corresponding to the parallel LAM, diagonal LAM, and cylindrical structures shown in Figs. 3(b), 3(c), and 3(e), respectively. The right shift of peaks in $g(r_{yz})$ curves suggests the NRs become more and more dispersed. Moreover, within the three phases (parallel LAM, diagonal LAM, and cylindrical), the corresponding values of average distance inter-NRs d_r are calculated to be $d_r = 2.26$, 2.43, and 2.55, respectively, which also indicates the NRs immersed in cylindrical phase are more dispersed than that in LAM phase. Moreover, although applied by shear, the NRs still

tend to be located within the preferential A domain. Additionally, the pair correlation function $g(r_{yz})$ for homopolymer (A_{10})/NRs composites at shear rates of $\dot{\gamma} = 0.01$, 0.06, and 0.09 are also depicted in the inset of Fig. 4, which also means that the dispersion of NRs is improved first as the shear rate $\dot{\gamma}$ increases, and consequently is stabilized at a high shear rate or even higher, which is in accordance with the simulations on the NPs dispersion in shear-flow polymer fluids.[9]

For the case of $\phi_{\rm R} = 30\%$, with the increase of shear rate $\dot{\gamma}$, the system also experiences the orientation and morphology transitions. Figures 5(a)–5(c) present three typical simulated pictures of nanocomposites at $\dot{\gamma}$=0, 0.05, and 0.15, corresponding to the initial ribbon, sheared cylindrical, and sheared ribbon structures, respectively, where NRs are still located within A domain. Detailed observation and comparison reveal that the shear-induced self-assembly of composites similarly experiences a symmetrical and reversible transition process: from initial ribbon to cylindrical phase with $\dot{\gamma}$ increasing from 0 to 0.05 shown in Figs. 5(a) and 5(b), and then conversely, from cylindrical to ribbon structure with $\dot{\gamma}$ increasing from 0.06 to 0.21 shown in Figs. 5(b) and 5(c).

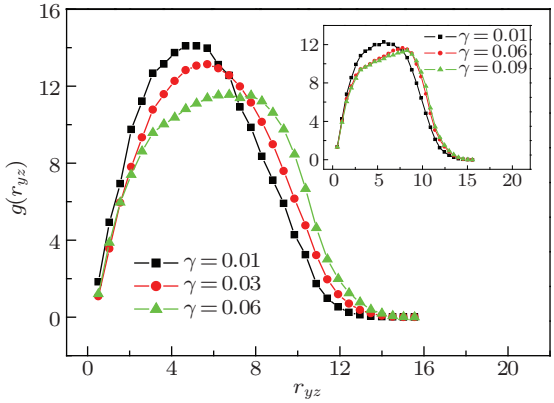
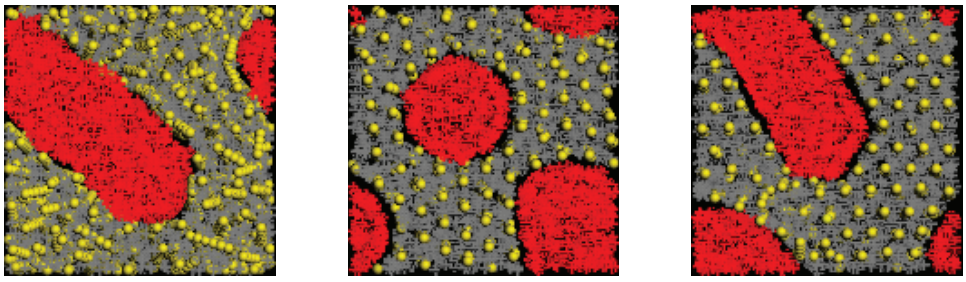


Fig. 4. (colour online) NR pair correlation function $g(r_{yz})$ for $\phi_{\rm R}$=15% at $\dot{\gamma}$=0.01, 0.03, and 0.06, corresponding to the parallel lamellar, diagonal lamellar, and cylindrical phases, respectively. The inset corresponds to the A_{10}/NR composites ($\phi_{\rm R} = 15\%$) at $\dot{\gamma} = 0.01$, 0.06, and 0.09.



(a) (b) (c)

Fig. 5. (colour online) Morphologies of DBCPs/NRs composites ($\phi_{\rm R} = 30\%$) at $\dot{\gamma} = 0$ (a), 0.05 (b), and 0.15 (c).

In Fig. 6, we also investigated the function relationship between shear viscosity η of the system and shear rate $\dot{\gamma}$ for the two cases of $\phi_{\rm R} = 15\%$ and $\phi_{\rm R} = 30\%$. Take $\phi_{\rm R} = 15\%$ for example, the curve with square points can be divided roughly into three regions, directly corresponding to the morphologies shown in Fig. 3. The first region corresponds to the low shear rates for $\dot{\gamma} < 0.05$, where the shear viscosity η decreases dramatically with shear rate increasing, followed by the two reorientations of transverse-to-parallel and transverse-to-diagonal shown in Figs. 3(b) and 3(c). Then, the shear viscosity η first increases and decreases again from $\dot{\gamma} = 0.05$ to 0.12 and displays the local convexes. Corresponding to Figs. 3(d) and 3(f), in this region no reorientations in LAM are induced, but the morphology transitions of lamellar-to-ribbon and lamellar-to-cylindrical structures are observed. After that, the shear viscosity η decreases gradually with shear rate in the third region increasing from $\dot{\gamma} = 0.13$ to 0.21, where the diagonal LAM is found again, and finally the perpendicular LAM phase is obtained, corresponding to Figs. 3(g) and 3(h). Generally, the shear viscosity η decreases as shear rate increases, corresponding to shear thinning, in which the layer width slightly decreases so that transverse LAM can take parallel or perpendicular orientations.[20] However, the local convexes in viscosity correspond to the shear-induced thickening, where the LAM is transformed into ribbon and cylindrical phase, whose width/diameter is larger than the width of the layer. For the case of $\phi_{\rm R} = 30\%$, it presents the same trend as for the case of $\phi_{\rm R} = 15\%$, which is clearly shown in Fig. 6.

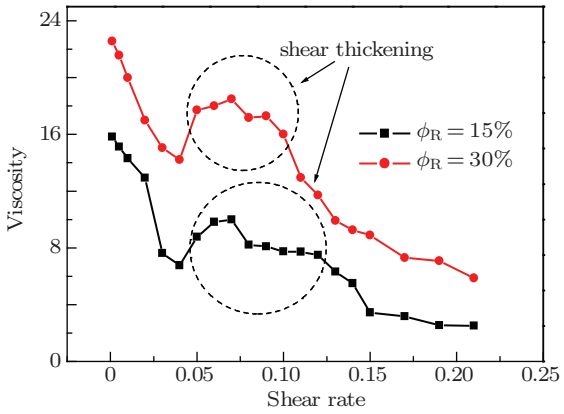


Fig. 6. (colour online) Values of shear viscosity η each as a function of shear rate.

Based on the above figures (Figs. 3–6), we can make a summary that the respective phase behaviours of shear-induced DBCP melts and NRs are co-responsible for the final morphology of composites. For pure DBCP melts, as the shear rate increases, the transverse LAM is oriented into a parallel alignment at low shear rates, and then reoriented into a perpendicular alignment at high shear rates. Fraser *et al.*[22] found that the perpendicular LAM is always associated with a lower potential energy, thus providing an energetic reason for favouring such a transition from transverse to perpendicular arrangement at higher shear rates. Moreover, the energetically favoured perpendicular LAM structure has a reduction in LAM spacing d_p compared with that of the parallel LAM structure, which is also in consistence with the previous results for high shear rates $\dot{\gamma}$, the shear flow reduces the LAM spacing.[23] For the case of pure NRs, we infer the two main influences of shear on NR phase behaviours. Firstly, shear guides the orientation of NRs to rapidly turn to shear direction; secondly, shear drives NRs to disperse with the increased average inter-rod distance d_r at low rates, and with the stabilized d_r at high rates. Finally, for the case of DBCPs/NRs mixtures, the final orientations and morphologies of composites depend on the competition between the two former phase behaviours. Also take $\phi_R = 15\%$ for example; at low shear rates from $\dot{\gamma} = 0$ to 0.02, both favoured parallel alignment of DBCPs and well shear-oriented NRs together help the system transform from transverse to parallel LAM. In the range from $\dot{\gamma} = 0.03$ to 0.06, on the one hand, the copolymers tend to adopt the perpendicular LAM with a lower potential energy; on the other hand, NRs tend to disperse within the preferential A domain. The latter is responsible mainly for phase transitions from transverse LAM to diagonal LAM, ribbon, and even cylindrical structures. Because the average inter-rod distance d_r of NRs dispersed in the preferential A domain increases, it equivalently enhances A-chain composition f_A, and then induces the phase transitions of lamellae-to-ribbon and lamellae-to-cylinder. Conversely, in a range from $\dot{\gamma} = 0.07$ to 0.12, the dispersion of NRs is not further enlarged, and meanwhile DBCPs still favour perpendicular LAM with lower potential energy and lower viscosity.[22] However, the time and the phase behaviours of DBCPs are responsible mainly for the reverse phase transitions from transverse LAM to cylindrical, ribbon, and diagonal LAM structures. The perpendicular LAM associated with shear thinning is manifested as a reduction in period spacing d_p, which narrows the dispersions of NRs, and equivalently reduces the composition f_A, and then induces the above reverse phase transitions. Finally, at high shear rates from $\dot{\gamma} = 0.13$ to 0.21, the perpendicular LAM is dominant for the final morphology of nanocomposites, with reducing layer spacing d_p, which not only narrows the NR distribution but also confines the orientation freedom of NRs within A domain, which has been suggested in Fig. 3(h). Finally, we can conclude that the shear can not only induce the orientation of self-assembled structure, but also arrange the ordered distribution of NRs in the polymer matrix.

3.3. High NRs concentration

Finally, we investigate the phase behaviours of DBCPs/NRs composites with a high NR concentration, $\phi_R = 35\%$, in comparison with the cases of low and moderate NR concentrations, respectively. As shown in Fig. 1(d), the initial phase of nanocomposites with $\phi_R = 35\%$ is typically cylindrical structure. Interestingly, as shear rate increases from $\dot{\gamma} = 0$ to 0.21, the cylindrical morphology is maintained in the entire range of shear rates, just followed by the reorientation of the cylindrical phase. Comparatively, figures 7(a) and 7(b) present the two typical pictures for DBCPs/NRs composites at shear rates of $\dot{\gamma} = 0$ and 0.05. There is no morphology transition, but only shear orients the cylindrical phase along the flow direction. As expected, shown in Fig. 7(b), NRs are also basically limited to the preferential A domain. Despite the cylindrical morphology maintained in the entire range of shear rates, the shear significantly influences the phase behaviours of NRs in two aspects:

spatial orientation and positional distribution. On the one hand, the NRs are oriented into the direction of shear flow, so only the head particles of rods are seen from Fig. 7(b). On the other hand, the shear regulates the distribution of NRs in the self-assembled DBCPs phase. To visualize the positional distribution of NRs within diblocks more clearly, the individual NRs are shown in Figs. 7(c) and 7(d), which are extracted from the self-assembled structures in Fig. 7(b). The NR superlattices in Fig. 7(c) demonstrate that the NRs with a high concentration applied by shear flow can assemble into ordered NRs arrays. Furthermore, as shown in Fig. 7(d), NRs are arranged in a hexagonal packing array, marked with connection lines between NR superlattices. The hexagon equivalently consists of three diamonds serving as basic cells, in each of which the natural ratio side length and diagonal length is $1 : \sqrt{3}$.

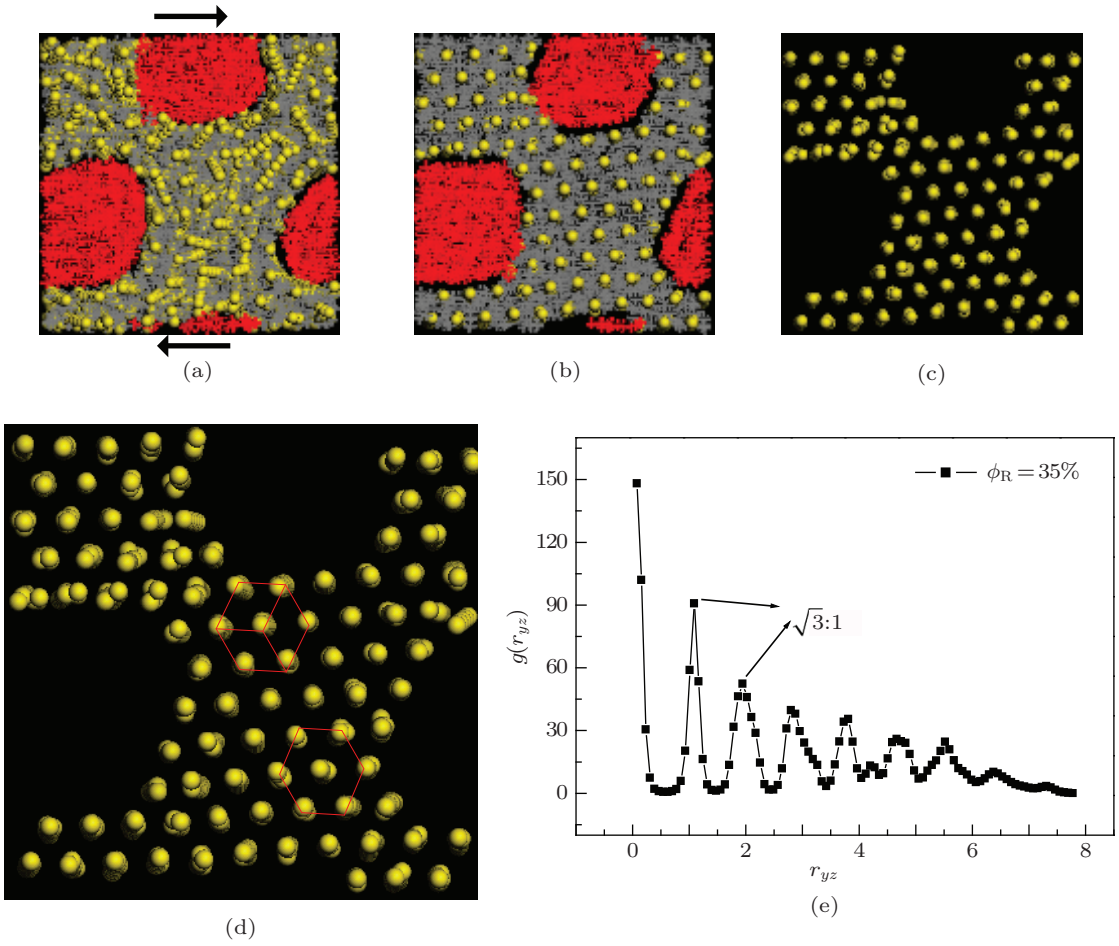


Fig. 7. (colour online) Morphologies of DBCPs/NRs composites ($\phi_R = 35\%$) at $\dot{\gamma} = 0$ (a) and 0.05 (b). NR superlattices with hexagonal packing array ((c) and (d)). NR pair correlation function $g(r_{yz})$ versus distance r_{yz} between NRs (e).

To obtain a more detailed insight into the lattice distribution of NRs in a diblock matrix, it is necessary to investigate the pair correlation function $g(r)$ between NRs. Figure 7(e) gives the 2D pair correlation function $g(r_{yz})$ as a function of distance r_{yz} between NRs. The first peak occurs at about $r_{yz} = 1.08$ (DPD units), and the second peak appears at about $r_{yz} = 1.87$ (DPD units), namely, their ratio of $1.87/1.08 = 1.73$ (approximately $1{:}\sqrt{3}$), is completely consistent with the natural side-to-diagonal ratio of the diamond as mentioned above. Figures 7(d) and 7(e) together confirm the 3D assembly of NRs arranged in a hexagonal close-packed structure, showing both orientational and positional order of NRs. A similar self-assembly of NRs into ordered arrays has been observed in a few recent experiments. For example, Mitamura *et al.*[24] fabricated the hydrophobic gold NRs, and investigated their 2D or 3D assembly in hexane solvent, which also depended on the concentration of NRs. At a high concentration, NRs

stood on the substrate and were arranged vertically in a hexagonal packing array. It was explained as follows: the interaction between NRs could be caused by the induced dipole moment in addition to the steric hindrance. Consequently, the dipole–dipole interaction was generated between adjacent NRs. In that case, the side-by-side interaction was more preferential than the edge-to-edge one since the induced dipole moments could be more effectively compensated in the former type.

Additionally, we indicate the effects of shear on the spatial orientation of NRs, which can be measured quantitatively as follows:

$$\langle P(\cos\theta)\rangle = \left\langle (3\cos^2\theta - 1)/2 \right\rangle, \tag{12}$$

where θ is the angle of NR orientation with respect to the shear direction (i.e., x-axis direction). The average NR orientation $\langle P(\cos\theta)\rangle$ will take values of -0.5, 0, and 1 for rods that are perpendicular, randomly oriented, and parallel to x axis respectively.[8] Figure 8 shows the values of average NR orientation $\langle P(\cos(\theta))\rangle$ each as a function of shear rate $\dot{\gamma}$ for different DBCPs/NRs systems with $\phi_{\rm R} = 5\%$, 15%, 30%, and 35%, respectively. Overall, as the shear rate increases from $\dot{\gamma} = 0$ to 0.21, the value of $\langle P(\cos(\theta))\rangle$ is stable at the former stage and decreases obviously at the latter stage. Specifically, take $\phi_{\rm R} = 15\%$ for example, corresponding to the morphologies of the system shown in Fig. 3, when shear rate $\dot{\gamma}$ is lower than 0.13, $\langle P(\cos(\theta))\rangle$ is nearly a constant of 1.0, indicating the NRs are well oriented to shear direction. Interestingly, when the shear rate increases up to 0.13 or even more, the value of $\langle P(\cos(\theta))\rangle$ then drops dramatically and finally decreases little with shear rate increasing. As expected, the NRs would be well oriented to the direction of applied shear, while here the NRs orientation $\langle P(\cos(\theta))\rangle$ decreases obviously at high shear rates, which suggests the orientation behaviours of NRs are interfered with by the shear-induced copolymer chains. As shear rate increases, the chains will be stretched, tilted, and even oriented. The stretched chains will energetically constrain the NR behaviour freedom, leading to a decrease in $\langle P(\cos(\theta))\rangle$. Moreover, from Fig. 8, it can be seen that the higher the NRs concentration, the less the influence of shear on NRs orientation is. It is attributed to the instinctive liquid crystalline behaviours from the anisotropic rods. However for the low NR concentration with $\phi_{\rm R} = 5\%$, the value of $\langle P(\cos(\theta))\rangle$ is more sensitive to the applied shear rate, indicating that NRs are dispersed in a diblock matrix with a relatively free orientation space.

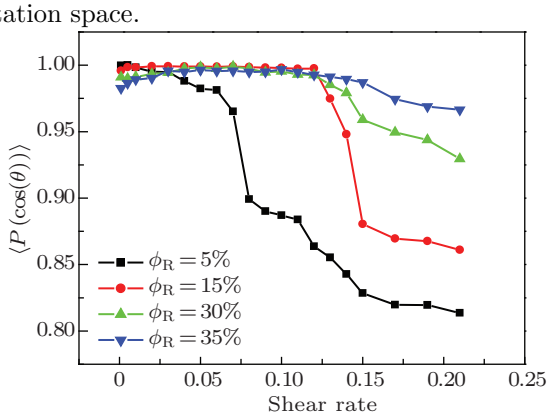


Fig. 8. (colour online) Values of average NR orientation $\langle P(\cos(\theta))\rangle$ each as a function of shear rate.

4. Conclusions

We have conducted DPD simulations to ascertain how steady shear affects the phase behaviours of lamellar diblock copolymer/nanorod composites. The rich orientation and morphology transitions are induced by the shear flow. We consider a wider range of NR concentrations, which is further divided into three cases: low, moderate, and high NR concentrations. Especially for the moderate NR concentration (such as $\phi_{\rm R} = 15\%$), the shear not only aligns the orientation of morphology along the shear flow, including the NRs, but also induces the composites to experience a symmetrical and reversible phase transition. The latter is determined by the competition between shear-induced NR dispersion and polymer thinning behaviours, also significantly depends on the concentration of NRs. For the high NR concentration (such as $\phi_{\rm R} = 35\%$), the morphology of composites is maintained but oriented to the shear flow, surprisingly, in which shear-induced NRs are arranged in hexagonal packing arrays. Meanwhile, the orientation behaviour of NRs in the block matrix is indicated by the average NR orientation $\langle P(\cos(\theta))\rangle$, which not only directly depends on applied shear, but also is significantly influenced by the shear-stretched alignment of chain molecules.

References

[1] Leibler L 1980 *Macromolecules* **13** 602

[2] Wang L, Chen X, Zhan J, Chai Y, Yang C, Xu L, Zhuang W and Jing B 2005 *J. Phys. Chem.* B **109** 3189

[3] Shankar S S, Rai A, Ahmad A and Sastry M 2005 *Chem. Mater.* **17** 566
[4] Kim F, Song J H and Yang P 2002 *J. Am. Chem. Soc.* **124** 14316
[5] Huynh W U, Dittmer J J and Alivisatos A P 2002 *Science* **295** 2425
[6] Zhang Q L, Gupta S, Emrick T and Russell T P 2006 *J. Am. Chem. Soc.* **128** 3898
[7] Tang Q and Ma Y 2009 *J. Phys. Chem.* B **113** 10117
[8] He L, Zhang L and Liang H 2010 *Polymer* **51** 3303
[9] Kalra V, Escobedo F and Joo Y L 2010 *J. Chem. Phys.* **132** 024901
[10] Mendoza C, Pietsch T, Gindy N and Fahmi A 2008 *Adv. Mater.* **20** 1179
[11] Pozzo D C and Walke L M 2007 *Macromolecules* **40** 5801
[12] He L, Pan Z Q, Zhang L and Liang H 2011 *Soft Matter* **7** 1147
[13] Groot R D and Madden T J 1998 *J. Chem. Phys.* **108** 8713
[14] AlSunaidi B A, den Otter W K and Clarke J H R 2004 *Phil. Trans. R. Soc. Lond.* **362** 773
[15] Allen M P and Tildesley D J 1987 *Computer Simulations of Liquids* (Oxford: Clarendon Press) p. 385
[16] Lees A W and Edwards S F 1972 *J. Phys.* C **5** 1921
[17] Matsen M W and Schick M 1994 *Phys. Rev. Lett.* **72** 2660
[18] Lee J Y, Thompson R B, Jasnow D and Balazs A C 2002 *Phys. Rev. Lett.* **89** 155503
[19] Koopi K A, Tirrell M F, Bates S, Almdal K and Colby R H 1992 *J. Phys.* II **2** 1941
[20] Lísal M and Brennan J K 2007 *Langmuir.* **23** 4809
[21] Satoh A, Chantrell R W, Kamiyama S and Coverdale G N 1996 *J. Colloid Interface Sci.* **181** 422
[22] Fraser B, Denniston C and Müser M H 2006 *J. Chem. Phys.* **124** 104902
[23] Rychkov I 2005 *Macromol. Theory Simul.* **14** 207
[24] Mitamura K, Imae T, Saito N and Takai O 2007 *J. Phys. Chem.* B **111** 8891